Experimental study on retardation of a heavy NAPL vapor in partially saturated porous media

Simon M. Kleinknecht[1], Holger Class[2], and Jürgen Braun[1]

[1]Facility for Subsurface Remediation, Institute for Modelling Hydraulic and Environmental Systems, University of Stuttgart, Pfaffendwaldring 61, 70569 Stuttgart, Germany

[2]Department of Hydromechanics and Modelling of Hydrosystems, Institute for Modelling Hydraulic and Environmental Systems, University of Stuttgart, Pfaffendwaldring 61, 70569 Stuttgart, Germany

Correspondence to: Simon M. Kleinknecht (simon.kleinknecht@iws.uni-stuttgart.de)

Abstract. NAPL contaminants introduced into the unsaturated zone spread as a liquid phase; however, they can also vaporize and migrate in a gaseous state. Vapor plumes migrate easily and, thus, pose a potential threat to underlying aquifers. Large-scale column experiments were performed to quantify partitioning processes responsible for the retardation of carbon disulfide (CS_2) vapor in partially saturated porous media. The results were compared with a theoretical approach taking into account the partitioning into the aqueous phase as well as adsorption to the solid matrix and to the air–water interface. The experiments were conducted in large, vertical columns (i.d. $= 0.109$ m) of 2 m length packed with different porous media. A slug of CS_2 vapor and the conservative tracer argon was injected at the bottom of the column followed by a nitrogen chase. Different seepage velocities were applied to characterize the transport and to evaluate their impact on retardation. Concentrations of CS_2 and argon were measured at the top outlet of the column using two gas chromatographs. The temporal-moment analysis for step input was employed to evaluate concentration breakthrough curves and to quantify dispersion and retardation. The experiments conducted showed a pronounced retardation of CS_2 in moist porous media which increased with water saturation. The comparison with an analytical solution helped to identify the relative contributions of partitioning processes to retardation. Thus, the experiments demonstrated that migrating CS_2 vapor is retarded as a result of partitioning processes. Moreover, CS_2 dissolved in the bulk water is amenable to biodegradation. First evidence of CS_2 decay by biodegradation was found in the experiments. The findings contribute to the understanding of vapor plume transport in the unsaturated zone and provide valuable experimental data for the transfer to field-like conditions.

1 Introduction

Subsurface contamination is a major concern in industrialized as well as in developing and emerging countries. NAPL contaminants introduced into the unsaturated zone spread as a liquid phase; however, they can also vaporize and migrate in a gaseous state. In particular, vapor (gas) plumes migrate easily in the unsaturated zone (Barber and Davis, 1991; Davis et al., 2005, 2009; Höhener et al., 2006; Brusseau et al., 2013). When assessing the danger of groundwater contamination by downward-migrating vapor plumes, retention effects on transport are of major interest. Processes such as dissolution into the bulk water or adsorption at interfaces affect the migration of vapors in the unsaturated zone. Vapor retardation could potentially slow down migration

and reduce the total contaminant mass eventually reaching, and thus endangering the groundwater. While fate and transport of vapor plumes have attracted a great deal of attention over the past years, further (contaminant-specific) investigations are necessary to improve the process understanding required to assess the threat to the environment (Rivett et al., 2011).

Carbon disulfide (CS_2) is a toxic, industrial, non-polar solvent among others used to manufacture viscose rayon. It is a dense non-aqueous phase liquid and highly volatile at standard conditions. Its vapor is characterized by a high density (1.6 times the air density) and is explosive. Hence, CS_2 vapor can migrate in the unsaturated zone, intrude into buildings, and distant ignition is possible. The U.S. Agency for Toxic Substances and Disease Registry ranks CS_2 168th on the Substance Priority List (SPL) of hazardous substances found on U.S. EPA National Priority List (NPL) sites (ATSDR, 2015). CS_2 has been found in 122 of the 1,844 sites on the NPL (USEPA, 2016). In addition, CS_2 has also been detected on CCl_4-contaminated sites as a result of abiotic degradation of CCl_4 (Davis et al., 2003).

Experimental studies (e.g. Brusseau et al., 1997; Kim et al., 1998; Costanza-Robinson et al., 2013) have been conducted to investigate retardation of the most common VOC in unsaturated porous media using short columns in the range of few decimeters and high flow velocities. Experimental results have been compared with standard as well as advanced advection-dispersion models (Popovičová and Brusseau, 1998; Toride et al., 2003). Corley et al. (1996) showed that low concentrations of volatile organic compounds distribute in the bulk phases (air, water and solid), adsorb to the air–water interface, and partition into intraparticle pores in unsaturated and saturated porous media. While it has been demonstrated in experiments that the gas-water interface poses a high potential for retardation (Brusseau et al., 1997; Costanza-Robinson and Brusseau, 2002b), determining the effective interfacial area, which controls the contaminant mass transfer, is still subject of intensive research (Goss, 2009; Kibbey and Chen, 2012; Brusseau et al., 2015). Mayes et al. (2003) stated that immobile water in pores could act as a short-term sink and as a long-term source of potential contaminants. The effect of moisture content on vapor retention has also been described by Cabbar and Bostanci (2001) and Maxfield et al. (2005) who discovered retardation to be negatively correlated to water saturation due to preferred adsorption on the solid matrix of certain components. The latter has additionally shown the dependency of retardation on the properties of the chemical component of interest. For instance, noble gases show no retardation at all. In summary, retardation of a contaminant vapor is a combination of different partitioning processes; their relative contribution depends on the physicochemical properties of the component as well as the properties of the porous medium (Costanza-Robinson et al., 2013).

The component- and porous-medium-dependent behavior of gas-phase retention emphasizes the need for a thorough investigation into retardation of carbon disulfide (CS_2) in partially saturated porous media. No detailed experimental studies on the retardation behavior of CS_2 vapor are available. Therefore, the first objective of this study was to design and conduct a large-scale column experiment to quantify retardation of CS_2 with clearly-defined and controlled boundary conditions. The experiments were conducted in vertical columns (i.d. = 0.109 m) of 2 m length packed with a porous medium. They were carried out under dry conditions and at static water saturations. Reproducible water saturations (initial conditions) were obtained by saturation with water and subsequent drainage under controlled conditions at predetermined capillary pressures. Tensiometers installed along the column were used to derive water-saturation profiles. A slug of CS_2 vapor and a non-retarding, conservative tracer (argon) was injected via an injection section at the bottom of the column. Velocities were varied in the range 25 to 200

Table 1. Characteristic properties of the porous media used for the experiments.

Parameter	Fine glass beads	Geba fine sand
Bulk density, kg m^{-3}	1420	1390
Grain size, mm	0.1 – 0.2	0.06 – 0.35
Permeability, m^2	1·10^{-11}	1·10^{-11}
Grain diameter d_{50}, μm	162	140
Pore diameter (median), μm	66	39
Smooth-sphere assumption SA, cm^{-1}	22.8	24.3
van Genuchten (constrained)		
α, cm^{-1}	0.0193	0.0145
n, dimensionless	17.783	10.305
θ_s, cm^3 cm^{-3}	0.392	0.460
θ_r, cm^3 cm^{-3}	0.043	0.071

cm h^{-1} in different experiments. Effluent concentrations of CS_2 and argon were measured online with gas chromatographs at the top outlet of the column. This set-up enabled for the quantification of CS_2 retardation as a function of porous medium, water saturation, and velocity. The second objective was to compare the experimental results with a theoretical approach, taking into account the different partitioning domains available for CS_2 and eventually responsible for retardation. This allowed to quantify contributions of the partitioning processes to total retardation. Hence, fundamental knowledge regarding the potential to delay or prevent a contamination of an underlying aquifer was gained.

2 Materials and methods

2.1 Experimental set-up

The experiments were conducted in vertical, stainless steel columns of 2 m length packed with two different types of porous media (Figure 1). The column (length = 2 m, i.d. = 0.109m) consisted of two custom-built, 1 m long sections. The ports along the column at a distance of 25 cm allowed for the installation of tensiometers to monitor capillary pressures. At the bottom of the column, the injection section with a base plate was installed. Into this base plate, a porous plate made of recrystallized silicon carbide was glued to act as a suction plate for the water drainage. The bottom of the column was realized as a constant-mass-flux boundary while the top is open to the surroundings, hence, at constant pressure.

Two different types of porous media (Table 1) were used in the experiments: fine glass beads (soda-lime glass, Sigmund Lindner, Warmensteinach, Germany) and Geba fine sand (Quarzsande GmbH, Eferding, Austria). Their grain-size distributions as well as capillary pressure - water saturation relationships are shown in Figure 2. Figure 3 shows scanning electron microscopy images of both materials illustrating their different shape and surface roughness. The columns were packed by
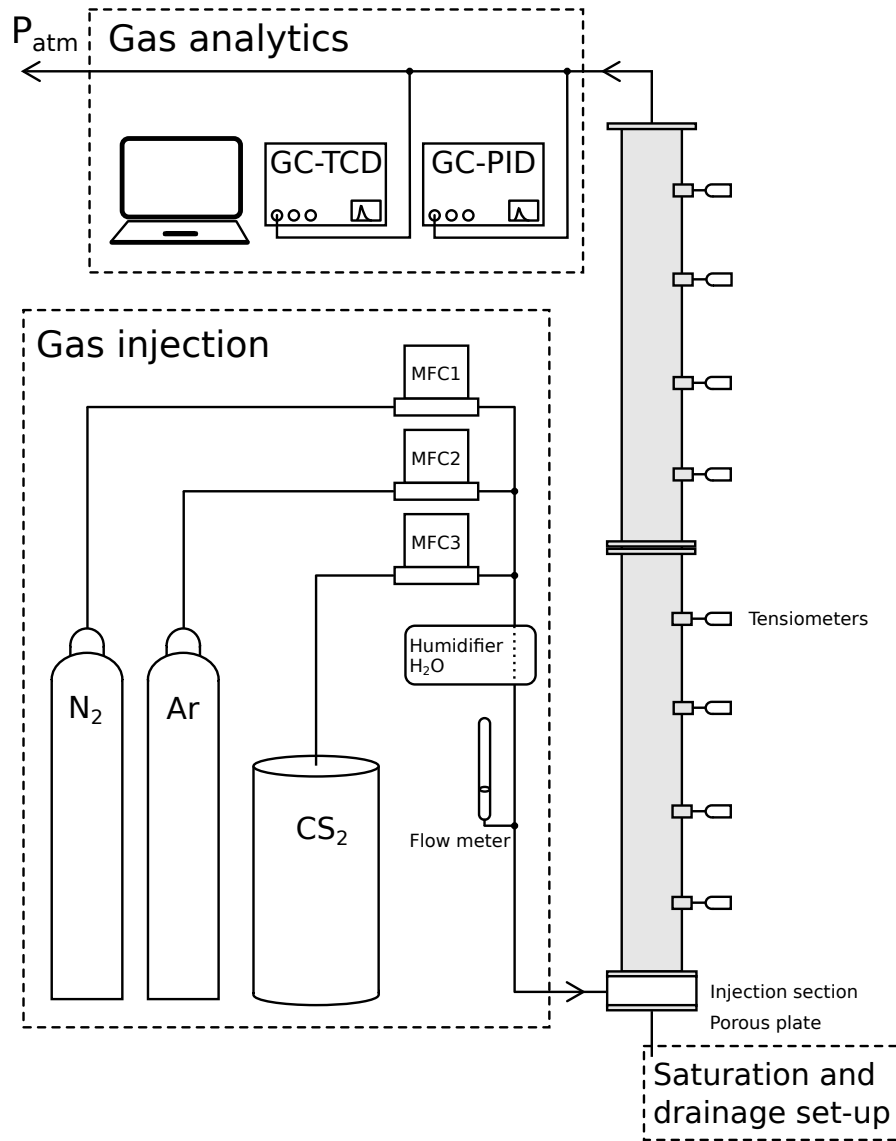
Figure 1. Flowchart of vapor-retardation experiment showing column, injection and saturation/drainage set-up.

dry pluviation using a sand rainer (Rad and Tumay, 1987; Lagioia et al., 2006). This ensured a homogeneous porous medium throughout. The columns were sealed with cover plates equipped with 1/8" tube fittings (SS-6M0-1-4RT, Swagelok). The experiments were carried out under dry conditions as well as at residual, static water saturation. Comparable initial conditions for each experiment were guaranteed by a set-up controlling and monitoring saturation and drainage. The drainage of the porous

5   media was realized by means of the porous plate at the bottom of the column exclusively permeable for water when fully saturated. This allowed for setting the water Table lower than the bottom of the column or flume. The saturations followed the
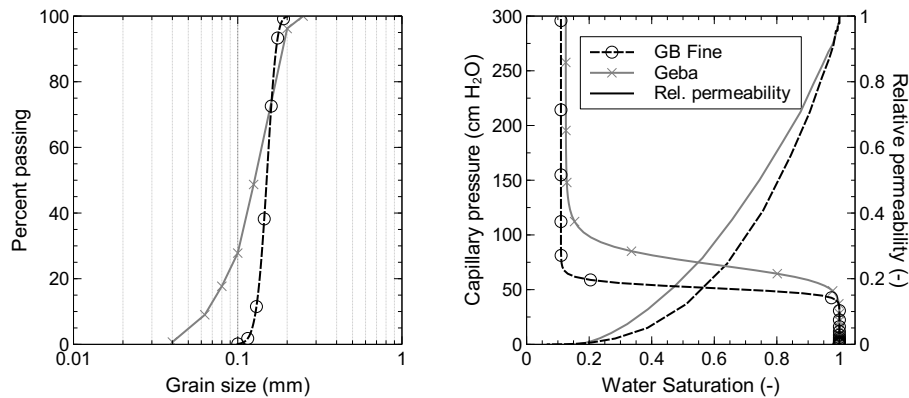
Figure 2. Grains-size distribution, capillary pressure–saturation relationship, and relative permeabilities (for the wetting phase) of materials used in experiments.
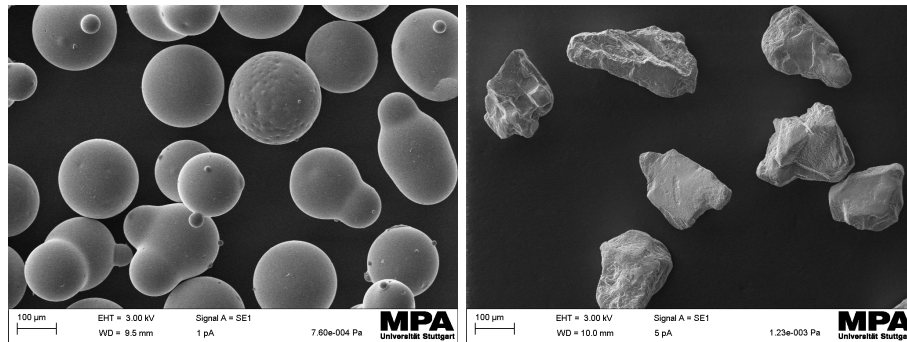
Figure 3. Scanning electron microscopy images of fine glass beads (left) and Geba fine sand (right) at a scale of 100 μm.

capillary pressure–saturation relationship (Fig. 2) measured in the laboratory. The water saturation was monitored using the tensiometers installed at the column ports. The tensiometer used for measuring capillary pressures consisted of a ceramic frit (length = 8 mm, o.d. = 6.5 mm, pore size = 2.5 um, porosity = 45 %, Porous Ceramics, Soilmoisture Equipment Corp., Santa Barbara, USA) glued in a stainless steel capillary (length = 200 mm, o.d. = 6 mm, i.d. = 4 mm). In addition, the column was
5   placed on a scale to permanently monitor its weight and thus the total amount of water.

    The injection section at the bottom of the column allowed for the injection of a gas-mixture slug at a predefined mass flux and, in addition, for a controlled upward flow stabilizing the vapor front. The CS_2 vapor was prepared prior to injection. Table 2 shows the physicochemical properties of the contaminant carbon disulfide (CS_2) at 20°C, 1013.15 hPa. A predefined amount of liquid CS_2 was injected into a barrel (V = 50 L) and pressurized to an excess pressure of about 2 bar with nitrogen to ensure
10   defined vapor properties. The tracer argon was provided from a gas cylinder (Westfalen AG, Münster, Germany). Constant mass fluxes of the injected CS_2 vapor and of the conservative tracer argon were critical to the experiment. Mass fluxes of argon, CS_2

Table 2. Physicochemical properties of contaminant carbon disulfide (CS_2) at $20°C$, $1013.15 \, hPa$.

Parameter	Value	Reference
CAS number	75-15-0	
Molecular weight (M_{CS2}), $g \, mol^{-1}$	76.1	Budavari (1996)
Density of liquid (ρ), $kg \, m^{-1}$	1263	Budavari (1996)
Solubility in water ($c_{w,sat}$), $g \, L^{-1}$	2.1	Riddick et al. (1986)
Henry constant (H_{cc}), dimensionless	1.04	Lide (2005)
Octanol-water partitioning coefficient ($log(K_{OW})$), dimensionless	2.00	USEPA, 1996
Organic-carbon partitioning coefficient (K_{OC}), $L \, kg^{-1}$	45.7	USEPA, 1996
Air–water partitioning coefficient (K_{IA}), cm	6.87×10^{-6}	Valsaraj (1988)
Boiling point (T_B), °C	46.5	Budavari (1996)
Vapor pressure (P_{sat}), hPa	396.9	Wagner equation
Saturation concentration in gas phase ($c_{a,sat}$), $kg \, m^{-3}$	1.239	Ideal gas law
Diffusion coefficient in air ($D_{CS_2 Air}$), $cm^2 \, s^{-1}$	9.71×10^{-2}	Chapman-Enskog

vapor, and nitrogen were controlled by mass-flow controllers (EL-FLOW, $Q_{max} = 3, 50$, and $10 \, mL \, m^{-1}$, Bronkhorst High-Tech B.V., Ruurlo, Netherlands). Complete gas tightness of the entire set-up was ensured by using 1/8" stainless steel capillaries throughout. The slug of the gas mixture (CS_2, argon ($Q_{Ar}/Q_{total} = 1.4 \, \%$), and carrier nitrogen) was injected and then pushed through the column using a nitrogen chase at the same flow rate. The nitrogen chase allowed to observe the contaminant recovery and the reversibility of partitioning processes.

In the case of moist experiments, the gas mixture slug was humidified with ultra-pure water (RH = 100 %) to avoid a drying-up of the moist porous medium. For the preparation of the gas-mixture slug, a custom-built miniature vaporizer (ICTV, University of Stuttgart, Germany) with an ultra-low volume pump (M6, VICI AG International, Schenkon, Switzerland) was used. The nitrogen used for the chase was bubbled through a gas scrubber filled with ultra-pure water. The inlet steel capillary loop (length = 4 m) and the scrubber were placed in a temperature-controlled water bath (Ministat 125, Huber Kältemaschinenbau GmbH, Germany) to minimize temperature-induced fluctuations during the experiments. The mass balance was closed based on the flow rate measured at the inflow, and the injection and effluent concentrations.

In the column outflow, CS_2 and argon concentration were measured to quantify retardation in dry and moist porous media. Two gas chromatographs were directly connected in-line to the column outlet. CS_2 concentrations were determined using a gas chromatograph with a photoionization detector (GC-PID HE1, Meta Messtechnische Systeme GmbH, Dresden, Germany) and argon concentrations were determined using a gas chromatograph with thermal conductivity detector (GC-TCD, Multiple gas analyzer 8610-0270, SRI Instruments Europe GmbH, Bad Honnef, Germany). Single-point calibrations were conducted prior to and after each run. Measurement intervals were set depending on the flow velocity such that a high temporal resolution (0.021 to 0.065 PV) of the breakthrough curves was obtained. Prior to the start of the slug injection, the concentration of CS_2

and argon in the slug mixture was measured as a base to normalize concentrations. A relative pressure transducer connected to the column inlet before the injection section was used to monitor the injection pressure. Since the top column outlet was open to the atmosphere (P_{atm}), this corresponded to the pressure loss caused by the flow through the porous medium. Temperature sensors and absolute pressure transducer continuously measured and recorded ambient and water bath temperature as well as atmospheric pressure in the vicinity of the experiment.

2.2 Experimental procedure

Various experiment series were conducted in two different porous media (fine glass beads and Geba fine sand) under both dry and partially saturated (moist) conditions. Within each series the columns were not repacked and no saturation-and-drainage cycle (SD) was carried out since first tests proved that the partitioning processes were fully reversible. The water saturation or total amount of water was monitored throughout the experiment. The slug of the gas mixture was injected with a predefined mass flux into the bottom of the 2 m long column such that it resulted in the designed seepage velocity. In each series, experiments were performed with different velocities including 25, 50, 100, and $200 \, \text{cm} \, \text{h}^{-1}$ (approx. 0.125, 0.25, 0.5, and $1.0 \, \text{PV} \, \text{h}^{-1}$) to observe kinetic effects on retardation. A slug of about 3.5 PV was used which corresponded to injection durations of approx. 3.5, 7, 14, and 28 h depending on the respective velocities. This ensured a residence time (plus safety factor) sufficient to attain steady-state conditions and for partitioning processes to reach equilibrium.

The experiments were conducted in four steps. In the first step, the flow rates (slug and chase) were adjusted to match the target seepage velocity. In the second step, the column was flushed with nitrogen. While maintaining constant flux, the inflow was switched to the slug injection of the gas mixture in the third step. After injecting 3.5 PV it was switched back to the nitrogen chase (fourth step).

2.3 Data evaluation

The quantification of retardation was based on gas concentration measurements of CS_2 and argon. Possible influences on the determined retardation factors due to experimental artifacts such as a deviation between theoretical and actual gas-effective pore volume had to be taken into consideration. Hence, for each experiment the breakthrough curve of CS_2 was related to that of argon. Concentrations were normalized with respect to the steady-state concentrations ($c = c_{exp}/c_{ss}$). Mass balance was calculated from concentration data and measured gas flow rates. Data was evaluated based on elapsed time and then correlated via flow rate, resulting from mass flux, to gas-effective pore volume. Breakthrough curves were evaluated using the temporal-moment analysis (TMA) for a step input (slug) as proposed by Yu et al. (1999) and Luo et al. (2006). The advantage of TMA "is that no underlying physical model is needed for calculating the travel times" (Yu et al. (1999), p. 3571), and the breakthrough curves of the CS_2-Ar mixture (slug front) as well as the nitrogen chase (slug tail) can be evaluated individually.

TMA was applied to obtain transport parameters (seepage velocity [Eq. A9] and dispersion coefficient [Eq. A10]) and mean breakthrough arrival (Eq. A7) time from concentration breakthrough curves. The retardation factor R of CS_2 vapor was

calculated from the ratio of the respective moments or mean breakthrough arrival time.

$$R = \frac{\tau_{CS_2}}{\tau_{Ar}} = \frac{M_{1,CS_2}}{M_{1,Ar}} \tag{1}$$

This ensured the independence from experimentally-induced deviations and thus allowed to delineate the impact of water saturation and velocity on retardation.

5   Retardation of a component can be estimated using analytical solutions based on experimental parameters and component-dependent coefficients for the different partitioning domains. Brusseau et al. (1997) showed that the theoretical retardation coefficient of a gaseous component in the unsaturated zone can be calculated with

$$R_t = 1 + \beta_w + \beta_s + \beta_{IA} = 1 + \frac{\theta_w}{\theta_a K_H} + \frac{\rho_b K_D}{\theta_a K_H} + \frac{K_{IA} A_{IA}}{\theta_a} \tag{2}$$

where θ_w is volumetric water content, θ_a is gas-filled porosity, K_H (dimensionless) is the Henry's constant, K_D (cm^3 g^{-1})
10   is the sorption coefficient for water-saturated conditions, ρ_b (g cm^{-3}) is the dry soil bulk density, K_{IA} (cm) is the adsorption coefficient at the gas-water interface, and A_{IA} (cm^2 cm^{-3}) is the specific surface area of the gas-water interface.

The coefficient K_D for CS$_2$ can be estimated with

$$K_D = K_{OC} \times f_{OC} \tag{3}$$

where K_{OC} (L kg^{-1}) is the soil organic carbon partitioning coefficient and f_{OC} is the fraction of organic carbon in the soil ma-
15   terial. The air–water partitioning coefficient K_{IA} of CS$_2$ can be estimated using empirical correlations between the interfacial-water partitioning constant K_{IW} and the octanol–water partitioning coefficient K_{OW} (Valsaraj, 1988).

$$K_{IW} = 3 \times 10^{-7} K_{OW}^{0.68} \tag{4}$$

$$K_{IA} = \frac{K_{IW}}{K_H} \tag{5}$$

20   The air–water interfacial area can be estimated with a correlation found by Costanza-Robinson et al. (2008) based on X-ray microtomography measurements of glass beads and natural sands.

$$A_{IA} = SA[(-0.9112)S_w + 0.9031] \tag{6}$$

where SA is the geometric surface area according to the smooth-sphere assumption (Tab. 1) and S_w is the water saturation.

3   Results and discussion

25   Column experiments were conducted with dry and moist porous media to characterize retardation of CS$_2$ vapor. Table 3 shows the experimental conditions of each series performed in fine glass beads and Geba fine sand. Several series of experiments were performed in each porous medium to quantify retardation. Series 1 refers to the experiments conducted in dry porous media

Table 3. Experimental conditions of vapor-retardation experiments in fine glass beads and Geba fine sand in dry and moist conditions (series).

Series	1	2	3	4
Condition	dry	moist	moist	moist
	Fine glass beads			
Porosity (ϕ)	0.40	0.40	0.40	0.40
Mean water saturation (S_w)	0.0	0.088	0.154	0.073
Eff. pore volume, L	7.72	7.04	6.53	7.16
	Geba fine sand			
Porosity (ϕ)	0.40	0.40	0.40	-
Mean water saturation (S_w)	0.0	0.162	0.150	-
Eff. pore volume, L	7.58	6.35	6.45	-

while Series 2 to 4 refer to the experiments in moist conditions. A saturation-and-drainage cycle was performed prior to each moist series. A slug of 3.5 PV of the gas mixture was injected ensuring, even for high flow rates, a sufficient residence time to reach equilibrium in the 2 m long column. Different velocities (25, 50, 100, and 200 cm h^{-1}) were applied, based on previously conducted experiments investigating density-driven vapor migration (Kleinknecht et al., 2015). Breakthrough curves under the prevailing experimental conditions were determined from concentration measurements at the column outlet. The temporal-moment analysis (Sec. 2.3) was applied to the breakthrough curves (BTC) to quantify diffusion/dispersion and retardation as a function of the porous media, the water saturation, and the flow conditions. A detailed summary of all experiments (experimental conditions, injected mass, and mass recovery) is given in Tables 5 and 6 in the appendix.

3.1 Water saturations

The moist porous medium required for this investigation was obtained by saturation and subsequent drainage via a suction plate. The capillary pressure was measured with tensiometers installed at the column ports to derive water saturations along the column (P$_c$–S$_w$, Fig. 2). Mean water saturations of the moist series are given in Table 3.

Figure 4 shows the initial water saturation profiles along the column measured in fine glass beads (only Series 4) and Geba fine sand (Series 2 and 3). Unfortunately, no tensiometer measurement data was available for Series 2 and 3 in fine glass beads. Thus the missing profiles have to be considered an element of uncertainty when evaluating retardation of CS$_2$ of these series. However, the available profile of Series 4 revealed a uniform saturation along the column, only slightly increasing toward the bottom from S$_w$ = 0.07 to 0.14. The very narrow and uniform grain-size distribution of the fine glass beads was responsible for a sharp transition from full to residual saturation (see P$_c$–S$_w$ curve in Fig. 2), thus favoring a uniform saturation profile. In Geba fine sand, a constant water saturation of S$_w$ = 0.15 above a column height of 70 cm was measured. However, both profiles showed a pronounced increase in the water saturation toward the bottom of the column, apparently reaching fully-saturated conditions according to the P$_c$–S$_w$ relationship of Geba fine sand (Fig. 2). Still, capillary pressures of P$_c$ = 55 and 65 hPa were
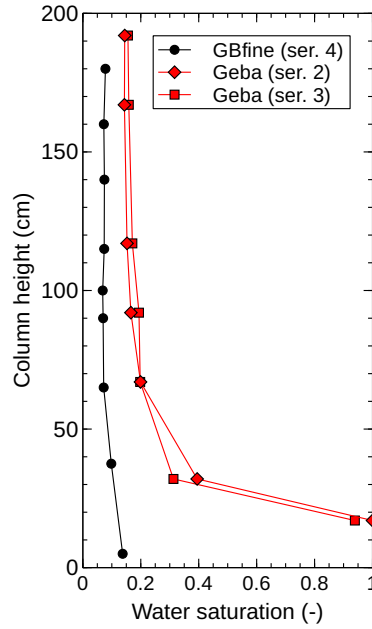
Figure 4. Initial water saturation.

measured at the lowest port. The suction applied via the porous plate was limited by its air entry pressure. A further decrease of pressure would have resulted in a breakthrough of air (continuous gas phase). The mean water saturation (Table 3) but also the observed profiles were expected to have an impact on the retardation behavior of CS_2, as discussed in Sec. 3.3.

A constant water-saturation profile in the porous medium was ensured by the humidification of all gases (gas-mixture slug and nitrogen chase) prior to injection. This was confirmed by a continuous weight measurement of the entire column throughout all experiments conducted within a series. Hence, the initial water-saturation profile could be maintained during the experiments.

3.2 Impact of velocity on breakthrough

Different migration velocities were applied to study their impact on the transport of argon and CS_2. Figure 5 shows breakthrough curves of CS_2 and argon as a function of pore volume for different flow conditions (velocities) in moist fine glass beads. The breakthrough curves were adapted to the actual gas-effective pore volume determined from the mean breakthrough arrival time τ_{Ar} (Eq. A7) of the conservative tracer argon. Seepage velocities of about 25, 50, 100, and 200 $\mathrm{cm\,h^{-1}}$ (residence time of about 8, 4, 2, and 1 h) were applied successively in the same column and under similar initial conditions. The lines represent measured concentrations (c/c_{ss}) normalized to steady-state concentration. The graphs are split and the right-hand side shows the outflow concentrations after the injection was switched from the gas-mixture slug to the nitrogen chase. The skewness of a BTC is a result of the longitudinal molecular diffusion and the mechanical mixing. The BTCs of argon and CS_2
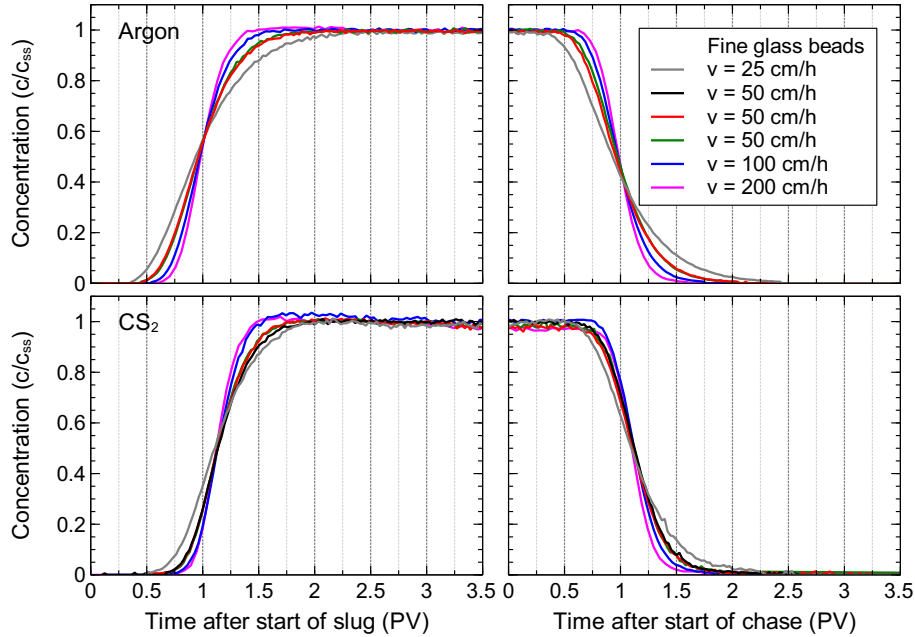
Figure 5. Breakthrough curves of CS_2 and Ar in moist fine glass beads ($S_w = 0.088$) for different velocities.

shown in the graphs illustrate that the skewness increased with decreasing seepage velocity as a result of diffusion during the longer residence time.

Dispersion coefficients were determined from temporal-moment analysis (TMA, see Sec. A3) of the breakthrough curves. Dispersion coefficients of argon and CS_2 increased from $D_{Ar} = 0.089$ to $0.142\,\mathrm{cm^2\,s^{-1}}$ and $D_{CS_2} = 0.033$ to $0.074\,\mathrm{cm^2\,s^{-1}}$ as a function of the seepage velocity. Under static conditions ($v = 0\,\mathrm{cm\,h^{-1}}$), the effective binary diffusion coefficients D^* in 5 porous media should apply. The effective binary diffusion coefficients D^* and the dispersivity α were determined based on a linear regression fitted to the dispersion coefficients as a function of the velocity for each porous medium. The y-intercepts of the regression lines represent the coefficient D^* and the slopes express dispersivity α of the respective porous medium. The theoretical coefficient D_t^* was determined according to the Chapman-Enskog theory and the approach by Millington and Quirk (1961) which accounts for tortuosity due to porous matrix and water saturation (see Sec. A1). Table 4 compares theoretical with 10 experimental effective binary diffusion coefficients of CS_2 and argon in fine glass beads and Geba fine sand under the given experimental conditions (water saturation S_w and tortuosity τ). The experimental coefficients D^* differed from the theoretical effective binary diffusion coefficient D_t^* calculated for the prevailing conditions. This could result from the choice of porous media, since both media were characterized by a uniform and narrow grain-size distribution, as well as the observed water-saturation profiles. Werner et al. (2004) reported that theoretical approaches are often sensitive since the majority of their 15 parameters are raised to a high power and do not apply satisfactorily to a wide variety of soils. Furthermore, the theoretical approach does not take into account material characteristics such as the pore-size distribution which may vary for similar

Table 4. Theoretical and experimental effective binary diffusion coefficient D^* of argon and CS_2, dispersivity α, and coefficient of determination R^2 of linear regression determined from experiments in moist porous media (Series 2).

Porous medium		Fine glass beads	Geba fine sand
Water saturation S_w		0.088	0.162
Tortuosity τ		0.220	0.161
Argon	D_t^*, cm^2 s^{-1}	0.0386	0.0284
	D^*, cm^2 s^{-1}	0.0909	0.0966
	α, cm	1.029	0.313
	R^2 (lin. regression)	0.919	0.254
CS$_2$	D_t^*, cm^2 s^{-1}	0.0213	0.0157
	D^*, cm^2 s^{-1}	0.0263	0.0332
	α, cm	0.888	0.552
	R^2 (lin. regression)	0.987	0.952

porosities and hence affect transport. In addition, the equation used to determine the dispersion coefficient (Eq. A10) from TMA raises the velocity to the power of three, thus minor deviations had a great impact on the final values.

The dispersivity α is a parameter of the porous medium only and should be independent of the components (gases) and flow conditions. A mean dispersivity of $\alpha_{\mathrm{GBfine}} = 0.958$ cm in fine glass beads and $\alpha_{\mathrm{Geba}} = 0.432$ cm in Geba fine sand was found. However, a difference between the dispersivity values of argon and CS_2 in the same porous medium was found in

5 the experiments (see Tab. 4) indicating that dispersivity is component dependent, due to e.g. diffusional or non-equilibrium effects. This component-dependent dispersivity has been shown by Costanza-Robinson and Brusseau (2002a), who reported that dispersivity ranges from approx. 0.1 to 5.0 cm. Hence, greater reliability was attributed to the dispersivity α_{Ar} determined from BTCs of argon since it is a conservative tracer.

3.3 Retardation of CS$_2$

10 Different series of experiments were conducted to quantify retardation of CS_2 as a function of water saturation and seepage velocity. Figure 6 and 7 compare breakthrough curves (BTC) of argon and CS_2 in dry (black) and moist (red) porous medium for the same seepage velocity (v = 50 cm h^{-1}). Two to three repetitions of each run in dry and moist conditions, respectively, are shown. The graphs show normalized concentrations as a function of effective pore volume (total pore volume minus water content after drainage).

15 The BTCs of argon showed excellent reproducibility in repetition experiments in both materials at the same conditions (v = 50 cm h^{-1}). In fine glass beads, argon showed very similar BTCs for dry and moist experiments. This thus confirmed that argon experiences no retardation and may be used as a conservative tracer and as a reference for CS_2. In Geba fine sand, a different skewness was observed between dry and moist conditions as a result of the reduced pore space in moist conditions.
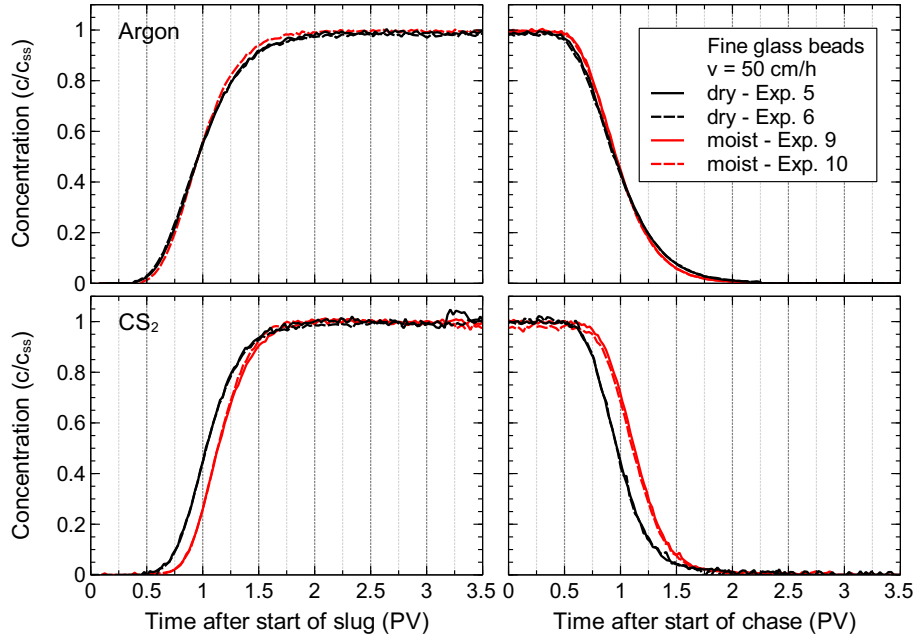
Figure 6. Breakthrough curves of CS_2 and Ar in dry and moist ($S_w = 0.088$) fine glass beads under identical slug and flow conditions (v = $50\,\mathrm{cm\,h^{-1}}$).

Hence, a comparison of the BTCs revealed that the effective-flow region in fine glass beads was similar in dry and moist conditions, whereas in Geba fine sand it was reduced in moist conditions. This resulted in BTCs which were less affected by diffusion due to a shorter residence time. Since the experiments were conducted with a constant-flow-rate boundary condition based on the calculated effective pore volume, a shorter residence time i.e. higher seepage velocity occurred when the actual effective pore volume available for gas flow is smaller than the calculated volume.

5  The BTCs of CS_2 showed, in general, good reproducibility for all experiments. In fine glass beads, a later breakthrough of CS_2 compared to argon can be observed in Figure 6, demonstrating the retardation of CS_2 due to partitioning processes. The different effective pore volume due to water and possible reduced residence time (actual vs. calculated PV) resulted in less skewed BTCs compared to the dry experiments. In Geba fine sand, a more pronounced retardation of CS_2 was observed compared to experiments in fine glass beads. The later breakthrough becomes evident when comparing BTCs in dry (black)

10 with moist (red) conditions in Figure 7. In two of the three BTCs in moist experiments (Fig. 7), CS_2 concentrations leveled at around $c/c_{ss} = 0.9$ followed by an increase to steady-state (plateau) concentrations toward the end of the slug. This behavior might be a consequence of the water saturation over column height affecting the partitioning processes.

  The retardation coefficients of CS_2 as a function of porous medium, water saturation, and seepage velocity were determined using the temporal-moment analysis (TMA) of the breakthrough curves (see Sec. 2.3). The coefficients were normalized with

15 respect to the BTCs from dry porous medium. Thereby, errors due to set-up or other systematic errors could be eliminated
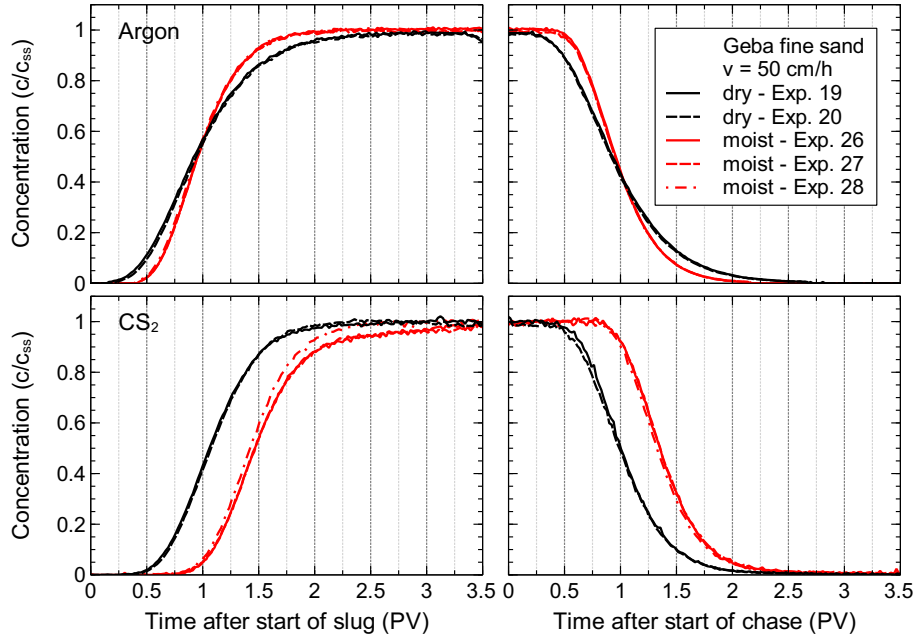
Figure 7. Breakthrough curves of CS_2 and Ar in dry and moist ($S_w = 0.154$) Geba fine sand under identical slug and flow conditions (v = 50 cm h^{-1}).

and allowed for the comparison with theoretical values. Figure 8 shows retardation coefficients of CS_2 as a function of water saturation (upper) and seepage velocity (lower) in fine glass beads (black) and Geba fine sand (red). The coefficients of the slug (circle) and the chase (rectangle) are given. Note the broken x-axis (water saturation) between $S_w = 0.10$ and 0.13 in the upper graph indicated by the vertical, dashed lines.

In fine glass beads, a non-linear increase in the retardation coefficient from $R_{GBfine} = 1.09$ to 1.16 with increasing water
5   saturation from $S_w = 0.075$ to 0.155 was observed. Of course, partitioning into the water phase and adsorption to the air–water interface depend on the interfacial area which should decrease with increasing water saturation. Thus an extrapolation of the retardation coefficient to higher water saturations might be difficult. The retardation of the slug and of the chase was different in fine glass beads, the chase being more prone to retardation than the slug. The breakthrough of the nitrogen chase (removal of the CS_2 vapor) showed a higher retardation by a factor (average) of 1.05 compared to the breakthrough of the slug throughout
10   all experiments in fine glass beads. This behavior can be also seen when comparing the BTCs of CS_2 in the upper graph of Figure 6.

In Geba fine sand, higher retardation coefficients compared to fine glass beads were measured in the experiments. These ranged between $R_{Geba} = 1.29$ and 1.34 at a mean water saturation of $S_w = 0.162$. This was due to the higher water saturation and its increase toward the bottom (discussed in Sec. 3.1), the different gas-water interfacial area, and the pore space available for
15   gas flow. Series 3 in Geba fine sand had to be excluded from these graphs due to mass balance issues discussed later. Hence,
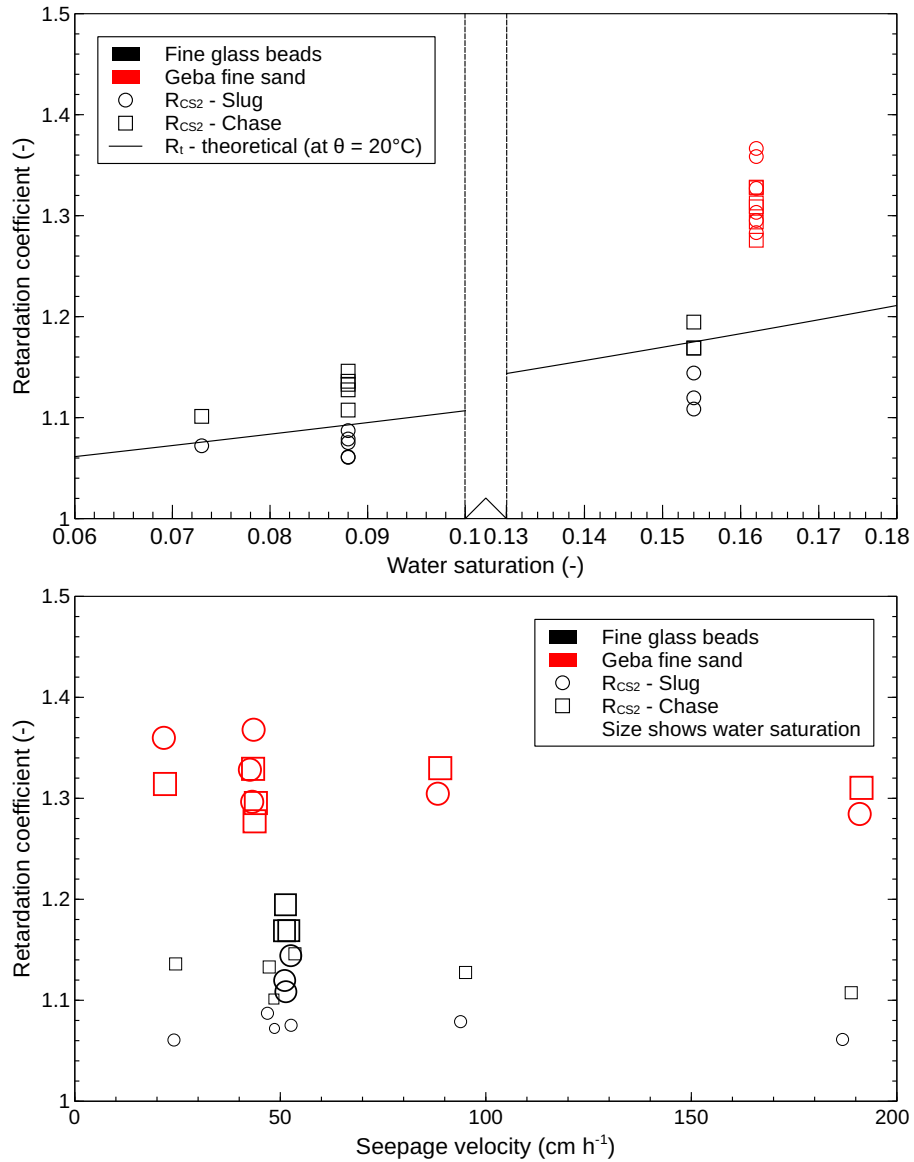
Figure 8. Retardation coefficients of CS_2 determined from experiments with different seepage velocities in fine glass beads and in Geba fine sand at different water saturations (evaluated with temporal-moment analysis).

results were only available for one particular water saturation profile in Geba fine sand. The ratio between the retardation coefficient of the slug and that of the chase did not show a clear trend as observed in fine glass beads despite the differences seen in Figure 8.

An evaluation of the processes responsible for retardation is possible utilizing the analytical solution (Eq. 2) proposed by Brusseau et al. (1997). The equation includes accumulation in the gas phase, partitioning into the aqueous phase, adsorption to

5   the solid phase, and adsorption to the gas-water interface. Partitioning into the aqueous phase (dissolution) is controlled by the temperature- and component-dependent Henry constant. Since equilibrium is assumed, the relative contribution of this process to the total retardation is considered as maximum.

Adsorption to the solid phase is governed by the partitioning coefficient K_D of that particular component. K_D is the product of the soil organic carbon partitioning coefficient K_{OC} and the fraction of organic carbon in the soil material f_{OC}. According to the Superfund Soil Screening Guidance (USEPA, 1996) for CS_2, the coefficient K_{OC} is 45.7 L kg^{-1}. Howard et al. (1990) reported that "carbon disulfide in solution would therefore not be expected to adsorb significantly to soil" due to the relatively low K_{OC}. The two types of materials used, fine glass beads and Geba fine sand, were evaluated with respect to organic carbon. The chemical composition of fine glass beads (soda-lime glass) is given by the manufacturer (Sigmund Lindner GmbH, SiLibeads Typ S 100 – 200 μm) as SiO_2 (72.5 %), Na_2O (13 %), CaO (9.1 %), MgO (4.2 %), and Al_2O_3 (0.58 %). Geba fine sand (Quarzsande GmbH, Geba weiss, 63 – 350 μm) is composed of SiO_2 (99.2 %), Fe_2O_3 (0.09 %), Al_2O_3 (1.85 %), and TiO_2 (0.24 %), thus a pure quartz sand. Both materials contain negligible fractions of organic carbon (f_{OC}), hence adsorption of CS_2 on the grains did not significantly contribute to retardation and may be neglected.

Adsorption on the air–water interface in a partially water-saturated porous medium depends on the air–water partitioning coefficient K_{IA} and on the air–water interfacial area A_{IA}. The air–water partitioning coefficient K_{IA} of CS_2 was estimated using the empirical correlation (Eq. 4 with Eq. 5) proposed by Valsaraj (1988). This correlation with $log(K_{OW}) = 2.00$ and the dimensionless Henry constant $K_H = 1.04$ yielded the air–water partitioning coefficient of CS_2 $K_{IA} = 6.87 \times 10^{-6} cm$. Costanza-Robinson et al. (2008) found a correlation (Eq. 6) based on on X-ray microtomography measurements of glass beads and natural sands to estimate the interfacial area. The calculated interfacial areas for a water saturation range from 0.05 to 0.20 decreases from 19.5 to 16.4 cm^{-1} for fine glass beads and from 20.9 to 17.5 cm^{-1} for Geba fine sand.

The theoretical retardation coefficient (Eq. 2) as a function of water saturation was calculated based on the assumptions, correlations and parameters discussed above. It is shown as a line in the upper graph of Figure 8. Only one line is plotted for both materials as the results are nearly identical due to similar porosities and calculated interfacial areas. In fine glass beads, the theoretical coefficient compared very well with the values from the experiments. It slightly overpredicted the retardation of the slug while it underpredicted that of the chase, however it reproduced satisfactorily the mean retardation coefficient and its increase with water saturation. In Geba fine sand, the theoretical coefficient, taking into account dissolution and adsorption to the air–water interface, significantly underestimated the observed retardation. The ratio between the contributions from dissolution β_w and from air–water interfacial adsorption β_{IA} at $S_w = 0.162$ yields $\beta_w/\beta_{IA} = 513$. Since dissolution, which is a function of the Henry constant and assumes equilibrium, is already at its maximum and adsorption to the grains may be neglected as discussed above, it is postulated that this increased retardation can only be caused by air–water interfacial adsorption. Possible reasons for an underestimation of the adsorption to the air–water interface could be that the inhomogeneous water saturation profiles (see Fig. 4), the grain-size distribution, or the underestimation of the specific surface of the Geba fine sand particles lead to an underestimation of the interfacial area. Scanning electron microscopy images (Fig. 3) suggested that the smooth-sphere assumption holds for glass beads but not necessarily for Geba fine sand, thus the interfacial area for Geba fine sand might have been significantly underestimated. Interfacial areas measured with microtomography are smaller than those

35   determined with vapor-phase tracer experiments (Brusseau et al., 2006; Costanza-Robinson et al., 2008). Furthermore, they reported that A_{IA} from microtomography measurements approach a maximum value similar to the smooth-sphere assumption while measurements from vapor-phase experiments rather approach a maximum close to the specific surface area of the material (BET measurements) as water saturation approaches zero. Costanza et al. (2000) observed the maximum interfacial area for water saturation in the range of 15 to 25 %. They also reported the possibility of multilayer adsorption and that the actual

5   adsorption may be significantly underestimated when true A_{IA} values are used.

    Attributing the observed discrepancy in Geba fine sand to air–water interfacial adsorption of CS_2, an interfacial area of about $A_{IA,calc} = 6553\,cm^{-1}$ would be required to obtain a mean retardation factor of $R_{Geba} = 1.31$. This is consistent with measured interfacial areas from vapor-phase tracer experiments (e.g. Costanza et al., 2000). Further experiments would be required using an additional tracer for air–water interfacial adsorption to actually measure the area and thereby quantify the relative

10   contribution of dissolution and interfacial adsorption to the total retardation of CS_2. The findings suggest that retardation may vary with changing saturation as a function of distance from groundwater table due to varying relative contributions of the partitioning processes. Since water saturations increase toward the groundwater table, more contaminant mass can partition into the bulk water phase but less mass is adsorbed to the air-water interface due to a reduced interfacial area.

    The lower graph in Figure 8 shows the retardation coefficients as a function of seepage velocity. A mean retardation coeffi-

15   cient of $R_{GBfine} = 1.100 \pm 0.0096$ and $R_{Geba} = 1.315 \pm 0.0152$ was measured in the experiments with fine glass beads ($S_w = 0.088$) and Geba fine sand ($S_w = 0.162$), respectively. In general, no significant change of the retardation behavior with increasing seepage velocity was observed. This confirmed that the mass transport rate was low enough and the residence time of the slug was sufficient for the partitioning processes to reach equilibrium. Concluding from the experiment with $v = 200\,\mathrm{cm\,h^{-1}}$ it seems likely that there was a slight tendency toward a reduced retardation. In fact, retardation may reduce at higher seepage velocities

20   due to limiting contaminant diffusion. If no equilibrium is reached in case of high velocities, the retardation coefficient reflects an apparent coefficient since in this case it is a function of the experimental system used (i.e. length of the column). Additional experimental repetitions would have been required to provide proof. However, this experimental investigation aimed at characterizing retardation of CS_2 in the range of velocities observed during vapor-plume migration experiments ($v \ll 200\,\mathrm{cm\,h^{-1}}$). Hence, the focus was laid on the velocities used and higher values were beyond the scope.

25   Mass balance analyses were performed to obtain mass recovery (r) from each breakthrough curve. Mass recovery was calculated from concentration and flow measurements and was normalized with respect to the injected mass. In general, mass recoveries of argon and CS_2 showed good results. Mean recovery calculated from all experiments conducted yielded for argon $r_{Ar} = 0.995 \pm 0.007$ and for CS_2 $r_{CS_2} = 0.981 \pm 0.084$ (excluding experiments of Series 3). Mass recoveries of all experiments are given in Tables 5 and 6 in the appendix. Complete mass recoveries proved reliability and quality of the results gained from

30   these column experiments.

    The results discussed above excluded Series 3 in Geba fine sand. Series 3 referred to the second saturation and drainage cycle which was carried out to establish a static water saturation different than in Series 2. However, significant CS_2 mass losses were observed and became more pronounced with each experiment in this series, eventually leading to its exclusion from the results. Recoveries of CS_2 decreased from $r_{CS_2} = 0.854$ in the first experiment of Series 3 down to $r_{CS_2} = 0.010$. This

mass loss of CS_2 was caused by biodegradation which was confirmed by the smell of hydrogen sulfide in the column outflow. The mass balance analysis of the experiments enabled for determining mean degradation rates of CS_2 which were calculated from the CS_2 mass rate and the recovery. The mean degradation rates ranged from 0.12 to $1.28\,\mathrm{mg\,h^{-1}}$ depending on the CS_2 mass flux applied in the experiments. Microbial degradation of CS_2 under aerobic and anaerobic conditions has been studied in the field of waste-gas treatment (e.g. Smith and Kelly, 1988; Hartikainen et al., 2000; Pol et al., 2007). They found microbes of the Thiobacillus species able to oxidize CS_2 under certain conditions. Cox et al. (2013) were the first to study degradation in soils and groundwater from a CS_2-contaminated site. They confirmed carbonyl sulfide (COS) and hydrogen sulfide (H_2S) as by-products and reported almost 100 % CS_2 degradation due to biological activity in their soil experiments. However, they also found evidence for microbial self-inhibition with increasing CS_2 concentration. This has been also reported by Pol et al. (2007) who additionally found inhibition of degradation due to accumulation of the intermediate products COS and H_2S. Hence, biodegradation is only relevant in specific environments and conditions and is most likely reduced as concentrations increase closer to the source zone of a contaminated site. This may explain why CS_2 is still persistent at many of the NPL sites listing CS_2 as a contaminant of concern.

A direct comparison with reported degradation rate constants determined from batch experiments could not be achieved due to the only availability of effluent gas concentrations in our experiments. Nonetheless, they showed that biodegradation may have a considerable potential for mitigating the contaminant mass transfer by vapor migration to the underlying aquifer, provided that favorable conditions for the specific microbes can be ensured, for instance via soil venting. A detailed investigation of biodegradation was beyond the scope of this work but should be addressed in future research.

4   Conclusions

– The retardation of CS_2 vapor was quantified in 2 m long column experiments in two different porous media as a function of water saturation and velocity by comparison with the conservative tracer argon. The temporal-moment analysis for a step-input (TMA) was applied to determine retardation factors and dispersion coefficients from concentration breakthrough curves. Comparison between experiments was achieved by relating mean arrival times of CS_2 to these of argon. The retardation coefficient of CS_2 increased from around 1.08 to 1.14 with increasing water saturation from 0.073 to 0.154 in fine glass beads. A slightly higher retardation of the chase by a factor of 1.05 compared to that of the slug was observed. A pronounced higher mean retardation of 1.31 was observed in Geba fine sand and a water saturation of 0.162 due to the different grain-size distribution and the particular water-saturation profile. Retardation coefficients as a function of (seepage) velocity revealed only a minor dependency and suggested a slight tendency toward a reduced retardation at higher velocities.

– The experimental retardation coefficients were compared to an analytical solution considering accumulation in the gas phase, partitioning to the aqueous phase, and adsorption to the air–water interface. Adsorption to the solid phase was neglected due to negligible fractions of organic matter in the porous media used. The analytic solution compared very well with the experimental results in fine glass beads identifying dissolution as the main contribution to retardation.

However, it underpredicted retardation in Geba fine sand. The discrepancy was ascribed to an increased relative contribution of air–water interfacial adsorption in Geba fine sand as a result of a significant underestimation of the interfacial area. They were estimated using a correlation derived from microtomography measurements of glass beads and natural soils and utilizing the smooth-sphere assumption (Costanza-Robinson et al., 2008). A readily applicable correlation to estimate interfacial areas is still considered a challenge and vapor-phase tracer experiments are so far the only reliable method to measure effective interfacial areas for vapor retardation. A quantification of the effective interfacial area could be achieved by using additional tracers which predominantly adsorb to the air–water interface.

– Clear evidence of the biodegradation of CS_2 was found in the last series of experiments in Geba fine sand confirmed by the concentration measurements and the mass balance analysis. These findings demonstrate the potential of biodegradation to reduce the total CS_2 mass of migrating vapor plumes eventually threating the underlying aquifer. Biodegradation of CS_2 has been confirmed by several experimental studies (e.g. Pol et al., 2007; Cox et al., 2013), however they showed that CS_2 degradation is only relevant in specific environments and conditions due to microbial self-inhibition at higher concentrations. Thus, site-specific investigations are needed to evaluate the potential for biodegradation or natural attenuation of a CS_2 contamination. Soil venting could be used to reduce self-inhibition and enhance biodegradation. The experiments showed a complete removal of the CS_2 vapor and a reversibility of partitioning processes confirmed by mass balance analyses. Vaporization rates of liquid CS_2 were not studied in this work and need to be investigated to estimate the removal efficiency of a liquid spill. Nevertheless a fast vaporization of liquid CS_2 is expected due to its low boiling point and high vapor pressure. This clearly supports the remediation of a CS_2 contamination in the unsaturated zone using soil-vapor extraction.

Data availability

The experimental data used to produce the results and graphs presented in this manuscript is available at http://dx.doi.org/10.4228/ZALF.2013.295 (Kleinknecht, 2016).

Appendix A: Materials and methods

A1   Binary diffusion coefficient

The Chapman-Enskog formula is used to estimate the binary diffusion coefficient of component A in B at low density.

$$D_{AB} = 1.8583 \times 10^{-3} \frac{\sqrt{T^3 \left(\frac{1}{M_A} + \frac{1}{M_B} \right)}}{p \sigma_{AB}^2 \Omega_{D,AB}} \qquad (A1)$$

with D_{AB} (cm^2 s^{-1}), temperature T (K), pressure p (atm), the Lennard-Jones parameter σ_{AB} (angstrom), and the collision integral $\Omega_{D,AB}$ which can be approximated with the Lennard-Jones potential. Component-specific values to determine σ_{AB} as well as $\Omega_{D,AB}$ as a function of kT/ϵ can be found in Bird et al. (1960).

Porous media affect diffusion of gases since space is occupied by grains and possibly by additional fluid phases. Therefore, Fick's law is often modified by the factor β to account for these deviations.

$$D^* = \beta D_{AB} \tag{A2}$$

while β is defined as

$$\beta = \phi S_g \tau \tag{A3}$$

where D^*_{AB} is the effective diffusion coefficient in porous media, ϕ is the porosity, S_g the gas saturation (equal to 1 for all-gas condition), and τ is the tortuosity. According to Millington and Quirk (1961), tortuosity can be approximated by

$$\tau = \phi^{1/3} S_g^{7/3} \tag{A4}$$

A2 Dispersion coefficient

Flow of fluids in a porous medium may vary significantly on a micro scale due to the velocity field in pores, irregularities of the pore size, flow restrictions, or dead-end pores resulting in additional spreading denoted as dispersion. These influences have to be taken into account in analytical or numerical solutions of flow in porous media. This is done by introducing the longitudinal dispersion coefficient

$$D = \beta D_{AB} + \alpha v = D^* + \alpha v \tag{A5}$$

with the dispersion coefficient D (cm^2 s^{-1}), effective binary diffusion coefficient D^*_{AB} (cm^2 s^{-1}) according to Eq. A2, gas-phase longitudinal dispersivity α (cm), and average gas velocity v (cm s^{-1}).

A3 Temporal-moment analysis

The measured breakthrough curve (BTC) data had to be prepared to allow for the usage of the temporal-moment analysis (TMA) generally applied to responses from dirac input. The breakthrough curves of the step-input boundary condition (1) were transformed to a dirac-input boundary condition (2) (Yu et al., 1999). This was achieved by using the derivative of the original step-input BTC data.

$$\frac{\partial c_1}{\partial t} = c_2 \tag{A6}$$

This transformation then allowed for analyzing the original breakthrough curves and required adapted definitions of the temporal moments. The first order normalized moment M_1 representing the mean breakthrough arrival time (τ) is then defined as

$$\tau = M_1 = \frac{m_1}{m_0} = \frac{\displaystyle\int_0^1 t \, dc_1}{\displaystyle\int_0^1 dc_1}, \tag{A7}$$

where c_1 (-) is normalized concentration of measured BTC and t (second or PV) is elapsed time. The second central moment μ_2 corresponds to the variance of travel times at the location of measurement and is given by

$$\mu_2 = \int_0^1 (t - M_1)^2 \, dc_1. \tag{A8}$$

These two moments can be used to directly infer seepage velocity v and dispersion coefficient D from BTC data for a one-dimensional system (Cirpka and Kitanidis, 2000).

$$v = \frac{z}{M_1} \tag{A9}$$

$$D = \frac{\mu_2 v^3}{2z} \tag{A10}$$

Appendix B: Detailed experimental results

Tables 5 and 6 show the theoretical seepage velocity, the injection duration (slug), the injected mass, and the normalized

10 recovery of the components CS_2 and argon. The tables list all experiments in order according to the conducted series.

Author contributions. Simon M. Kleinknecht designed and conducted this experimental study. Holger Class and Jürgen Braun were responsible for the scientific and experimental supervision. Simon M. Kleinknecht prepared the manuscript with contributions from both co-authors. The authors declare that they have no conflict of interest.

Table 5. Experimental conditions of vapor-retardation experiments in fine glass beads: series, experiment, theoretical seepage velocity, injection duration, and injected mass and recovery of CS_2 and argon.

Series	Exp.	v	t_{inj}	m_{Ar}	m_{CS2}	r_{Ar}	r_{CS2}
#	#	$cm\,h^{-1}$	h	mg	mg	-	-
Fine glass beads							
1	1	25	27.80	667.8	2671.4	0.994	1.123
	2	50	13.92	677.7	2710.9	1.011	1.066
	3	50	14.10	675.9	2703.5	0.996	1.005
	4	50	13.65	677.7	542.2	0.992	1.033
	5	50	14.29	690.3	13.8	0.988	0.822
	6	50	14.07	687.0	13.7	0.984	0.753
	7	50	13.82	673.3	13.5	0.987	0.770
2	8	25	28.35	619.9	12.4	0.989	1.022
	9	50	14.40	617.8	12.4	0.993	0.983
	10	50	12.83	615.2	12.3	0.997	1.010
	11	100	7.22	620.8	12.4	1.000	0.941
	12	200	3.56	617.1	12.3	0.998	0.941
3	13	50	14.38	635.0	12.7	0.995	1.054
	14	50	14.22	634.0	12.7	1.000	1.032
	15	50	14.43	635.4	12.7	0.989	1.013
4	16	50	14.06	626.0	12.5	0.994	1.039

Table 6. Experimental conditions of vapor-retardation experiments in Geba fine sand: series, experiment, theoretical seepage velocity, injection duration, and injected mass and recovery of CS_2 and argon.

Series	Exp.	v	t_{inj}	m_{Ar}	m_{CS2}	r_{Ar}	r_{CS2}
#	#	$cm\,h^{-1}$	h	mg	mg	-	-
Geba fine sand							
1	17	25	28.71	673.9	13.5	0.982	0.964
	18	25	40.97	944.5	18.9	0.992	0.942
	19	50	14.30	599.2	12.0	0.985	1.006
	20	50	14.31	597.5	12.0	0.983	0.970
	21	100	7.20	664.8	13.3	0.999	0.994
	22	100	7.32	665.9	13.3	0.999	1.062
	23	200	3.83	706.2	14.1	1.000	0.994
	24	200	3.54	657.7	13.2	0.995	0.962
2	25	25	41.17	795.7	15.9	0.984	1.009
	26	50	14.33	552.8	11.1	1.000	0.955
	27	50	20.28	767.3	15.3	0.992	1.115
	28	50	20.62	799.5	16.0	0.997	0.973
	29	100	10.12	797.6	16.0	0.987	0.965
	30	200	4.67	800.8	16.0	1.000	1.013
3	31	50	20.54	815.8	16.3	0.994	0.854
	32	50	24.04	955.8	19.1	0.998	0.684
	33	100	11.02	864.1	17.3	1.000	0.534
	34	200	5.16	782.9	15.7	1.008	0.689
	35	25	49.26	957.3	19.1	1.012	0.010
	36	100	10.28	793.0	15.9	1.000	0.174
	37	50	23.81	944.0	18.9	0.996	0.016

References

Barber, C. and Davis, G. B.: Fugacity model to assess the importance of factors controlling the movement of volatile organics from soil to ground water, in: Proceedings of a Workshop on Modelling the Fate of Chemicals in the Environment, pp. 67–73, The Australian National University, Centre for Resource and Environmental Studies, Water Research Foundation of Australia, 1991.

Bird, R. B., Stewart, W. E., and Lightfoot, E. N.: Transport phenomena, Wiley, New York, 1960.

5 Brusseau, M. L., Popovičová, J., and Silva, J. A. K.: Characterizing gas-water interfacial and bulk-water partitioning for gas-phase transport of organic contaminants in unsaturated porous media, Environmental Science & Technology, 31, 1645–1649, doi:10.1021/es960475j, 1997.

Brusseau, M. L., Peng, S., Schnaar, G., and Costanza-Robinson, M. S.: Relationships among air-water interfacial area, capillary pressure, and water saturation for a sandy porous medium, Water Resources Research, 42, n/a–n/a, doi:10.1029/2005WR004058, http://dx.doi.org/10.1029/2005WR004058, w03501, 2006.

Brusseau, M. L., Carroll, K. C., Truex, M. J., and Becker, D. J.: Characterization and Remediation of Chlorinated Volatile Organic Contaminants in the Vadose Zone, Vadose Zone Journal, 12, –, doi:10.2136/vzj2012.0137, http://dx.doi.org/10.2136/vzj2012.0137, 2013.

Brusseau, M. L., Ouni, A. E., Araujo, J. B., and Zhong, H.: Novel methods for measuring air–water interfacial area in unsaturated porous media, Chemosphere, 127, 208 – 213, doi:http://dx.doi.org/10.1016/j.chemosphere.2015.01.029, http://www.sciencedirect.com/science/article/pii/S0045653515000697, 2015.

Budavari, S., ed.: The Merck index: an encyclopedia of chemicals, drugs, and biologicals, Merck, Whitehouse Station, NJ, 12. edn., http://www.gbv.de/dms/ohb-opac/198126255.pdf, 1996.

Cabbar, H. and Bostanci, A.: Moisture effect on the transport of organic vapors in sand, Journal of Hazardous Materials, 82, 313–322, doi:10.1016/S0304-3894(01)00177-7, http://www.sciencedirect.com/science/article/pii/S0304389401001777, 2001.

20 Cirpka, O. A. and Kitanidis, P. K.: Characterization of mixing and dilution in heterogeneous aquifers by means of local temporal moments, Water Resources Research, 36, 1221–1236, doi:10.1029/1999WR900354, http://dx.doi.org/10.1029/1999WR900354, 2000.

Corley, T. L., Farrell, J., Hong, B., and Conklin, M. H.: VOC accumulation and pore filling in unsaturated porous media, Environmental Science & Technology, 30, 2884–2891, doi:10.1021/es950644k, 1996.

Costanza, M. S., , and Brusseau, M. L.: Contaminant Vapor Adsorption at the Gas–Water Interface in Soils, Environmental Science & Technology, 34, http://pubs.acs.org/doi/abs/10.1021/es9904585, 2000.

Costanza-Robinson, M. S. and Brusseau, M. L.: Gas phase advection and dispersion in unsaturated porous media, Water Resources Research, 38, 7–1–7–9, doi:10.1029/2001WR000895, 2002a.

Costanza-Robinson, M. S. and Brusseau, M. L.: Air-water interfacial areas in unsaturated soils: Evaluation of interfacial domains, Water Resour. Res., 38, 13–1–13–17, http://dx.doi.org/10.1029/2001WR000738, 2002b.

30 Costanza-Robinson, M. S., Harrold, K. H., and Lieb-Lappen, R. M.: X-ray Microtomography Determination of Air–Water Interfacial Area–Water Saturation Relationships in Sandy Porous Media, Environ. Sci. Technol., 42, 2949–2956, doi:10.1021/es072080d, http://pubs.acs.org/doi/abs/10.1021/es072080d, 2008.

Costanza-Robinson, M. S., Carlson, T. D., and Brusseau, M. L.: Vapor-phase transport of trichloroethene in an intermediate-scale vadose-zone system: Retention processes and tracer-based prediction, Journal of Contaminant Hydrology, 145, 82–89, doi:10.1016/j.jconhyd.2012.12.004, http://www.sciencedirect.com/science/article/pii/S0169772212001696, 2013.

Cox, S. F., McKinley, J. D., Ferguson, A. S., O'Sullivan, G., and Kalin, R. M.: Degradation of carbon disulphide (CS2) in soils and groundwater from a CS2-contaminated site, Environmental Earth Sciences, 68, 1935–1944, doi:10.1007/s12665-012-1881-y, http://dx.doi.org/10.1007/s12665-012-1881-y, 2013.

Davis, A., Fennemore, G., Peck, C., Walker, C., McIlwraith, J., and Thomas, S.: Degradation of carbon tetrachloride in a reducing groundwater environment: implications for natural attenuation, Applied Geochemistry, 18, 503 – 525, doi:http://dx.doi.org/10.1016/S0883-2927(02)00102-6, http://www.sciencedirect.com/science/article/pii/S0883292702001026, 2003.

Davis, G., Patterson, B., and Trefry, M.: Evidence for Instantaneous Oxygen-Limited Biodegradation of Petroleum Hydrocarbon Vapors in the Subsurface, Ground water monitoring & remediation, 29, 126–137, doi:10.1111/j.1745-6592.2008.01221.x, 2009.

Davis, G. B., Rayner, J. L., Trefry, M. G., Fisher, S. J., and Patterson, B. M.: Measurement and modeling of temporal variations in hydrocarbon vapor behavior in a layered soil profile, Vadose Zone Journal, 4, 225–239, doi:10.2136/vzj2004.0029, https://dl.sciencesocieties.org/publications/vzj/abstracts/4/2/225, 2005.

for Toxic Substances, A. and Registry, D.: Priority List of Hazardous Substance, https://www.atsdr.cdc.gov/spl/, 2015.

Goss, K.-U.: Predicting Adsorption of Organic Chemicals at the Air−Water Interface, The Journal of Physical Chemistry A, 113, 12 256–12 259, doi:10.1021/jp907347p, pMID: 19803507, 2009.

Hartikainen, T., Ruuskanen, J., Räty, K., von Wright, A., and Martikainen, P.: Physiology and taxonomy of Thiobacillus strain TJ330, which oxidizes carbon disulphide (CS2), Journal of Applied Microbiology, 89, 580–586, doi:10.1046/j.1365-2672.2000.01150.x, 2000.

Höhener, P., Dakhel, N., Christophersen, M., Broholm, M., and Kjeldsen, P.: Biodegradation of hydrocarbons vapors: comparison of laboratory studies and field investigations in the vadose zone at the emplaced fuel source experiment, Airbase Værløse, Denmark, Journal of Contaminant Hydrology, 88, 337–358, doi:10.1016/j.jconhyd.2006.07.007, http://www.sciencedirect.com/science/article/pii/S0169772206001343, 2006.

Howard, P., Sage, G., Jarvis, W., and Gray, D.: Handbook of environmental fate and exposure data for organic chemicals. Volume II: Solvents, Chelsea, MI (US); Lewis Publishers, Inc., 1990.

Kibbey, T. C. G. and Chen, L.: A pore network model study of the fluid-fluid interfacial areas measured by dynamic-interface tracer depletion and miscible displacement water phase advective tracer methods, Water Resources Research, 48, n/a–n/a, doi:10.1029/2012WR011862, http://dx.doi.org/10.1029/2012WR011862, w10519, 2012.

Kim, H., Annable, M. D., and Rao, P. S. C.: Influence of air-water interfacial adsorption and gas-phase partitioning on the transport of organic chemicals in unsaturated porous media, Environmental Science & Technology, 32, 1253–1259, doi:10.1021/es970868y, 1998.

Kleinknecht, S.: Data sets of experimental study on retardation of a heavy NAPL vapor in partially saturated porous media, Leibniz-Zentrum für Agrarlandschaftsforschung (ZALF) e.V., doi:10.4228/ZALF.2013.295, 2016.

Kleinknecht, S. M., Class, H., and Braun, J.: Density-driven migration of heavy NAPL vapor in the unsaturated zone, Vadose Zone Journal, 14, doi:10.2136/vzj2014.12.0173, http://dx.doi.org/10.2136/vzj2014.12.0173, 2015.

Lagioia, R., Sanzeni, A., and Colleselli, F.: Air, water and vacuum pluviation of sand specimens for the triaxial apparatus, Soils And Foundations, 46, 61–67, doi:10.3208/sandf.46.61, 2006.

Lide, D. R.: CRC Handbook of chemistry and physics, CRC Press, 86 edn., 2005.

Luo, J., Cirpka, O. A., and Kitanidis, P. K.: Temporal-moment matching for truncated breakthrough curves for step or step-pulse injection, Advances in Water Resources, 29, 1306–1313, doi:10.1016/j.advwatres.2005.10.005, http://www.sciencedirect.com/science/article/pii/S0309170805002496, 2006.

Maxfield, B. T., Ginosar, D. M., McMurtrey, R. D., Rollins, H. W., and Shook, G. M.: The effect of moisture content on retention of fluorocarbon tracers on sand, Geothermics, 34, 47–60, doi:10.1016/j.geothermics.2004.06.003, http://www.sciencedirect.com/science/article/pii/S0375650504000392, 2005.

Mayes, M., Jardine, P., Mehlhorn, T., Bjornstad, B., Ladd, J., and Zachara, J.: Transport of multiple tracers in variably saturated humid region structured soils and semi-arid region laminated sediments, Journal of Hydrology, 275, 141–161, doi:10.1016/S0022-1694(03)00039-8, http://www.sciencedirect.com/science/article/pii/S0022169403000398, 2003.

Millington, R. J. and Quirk, J. P.: Permeability of porous solids, Transactions of the Faraday Society, 57, 1200–1207, doi:10.1039/TF9615701200, 1961.

Pol, A., van der Drift, C., and Op den Camp, H.: Isolation of a carbon disulfide utilizing Thiomonas sp. and its application in a biotrickling filter, Applied Microbiology and Biotechnology, 74, 439–446, doi:10.1007/s00253-006-0663-4, 2007.

Popovičová, J. and Brusseau, M. L.: Contaminant mass transfer during gas-phase transport in unsaturated porous media, Water Resources Research, 34, 83–92, doi:10.1029/97WR02945, 1998.

Rad, N. and Tumay, M.: Factors affecting sand specimen fabrication by raining, Geotechnical Testing Journal, 10, 31–37, doi:10.1520/GTJ10136J, 1987.

Riddick, J. A., Bunger, W. B., and Sakano, T. K.: Organic Solvents: Physical Properties And Methods Of Purification, vol. XV, Wiley, New York, 4th edn., http://www.gbv.de/dms/ilmenau/toc/01792670X.PDF, 1986.

Rivett, M. O., Wealthall, G. P., Dearden, R. A., and McAlary, T. A.: Review of unsaturated-zone transport and attenuation of volatile organic compound (VOC) plumes leached from shallow source zones, Journal of Contaminant Hydrology, 123, 130–156, doi:10.1016/j.jconhyd.2010.12.013, http://www.sciencedirect.com/science/article/B6V94-51XH94M-1/2/000e9c8578e4476286054f5b05ca15e4, 2011.

Smith, N. A. and Kelly, D. P.: Oxidation of Carbon Disulphide as the Sole Source of Energy for the Autotrophic Growth of Thiobacillus thioparus Strain TK-m, Microbiology, 134, 3041–3048, http://mic.microbiologyresearch.org/content/journal/micro/10.1099/00221287-134-11-3041, 1988.

Toride, N., Inoue, M., and Leij, F. J.: Hydrodynamic dispersion in an unsaturated dune sand, Soil Science Society of America Journal, 67, 703–712, doi:10.2136/sssaj2003.0703, https://www.soils.org/publications/sssaj/abstracts/67/3/703, 2003.

U.S. Environmental Protection Agency: Superfund Soil Screening Guidance – Technical Background Document – Part 5: Chemical-Specific Parameters, Tech. rep., Office of Solid Waste and Emergency Response, https://semspub.epa.gov/work/HQ/175235.pdf, 1996.

U.S. Environmental Protection Agency: National Priority List (NPL): advanced query form, https://cumulis.epa.gov/supercpad/cursites/srchsites.cfm, 2016.

Valsaraj, K. T.: On the physico-chemical aspects of partitioning of non-polar hydrophobic organics at the air-water interface, Chemosphere, 17, 875 – 887, doi:http://dx.doi.org/10.1016/0045-6535(88)90060-4, http://www.sciencedirect.com/science/article/pii/0045653588900604, 1988.

Werner, D., Grathwohl, P., and Höhener, P.: Review of field methods for the determination of the tortuosity and effective gas-phase diffusivity in the vadose zone, Vadose Zone Journal, 3, 1240–1248, doi:10.2136/vzj2004.1240, http://dx.doi.org/10.2136/vzj2004.1240, 2004.

Yu, C., Warrick, A. W., and Conklin, M. H.: A moment method for analyzing breakthrough curves of step inputs, Water Resources Research, 35, 3567–3572, doi:10.1029/1999WR900225, http://dx.doi.org/10.1029/1999WR900225, 1999.